ADVANCED MATERIALS INTERFACES
Open Access
www.advmatinterfaces.de

Triarylamine Trisamide Interfacial Modulation for Perovskite Photovoltaics

Masaud Almalki, Ghewa AlSabeh, Marco A. Ruiz-Preciado, Hong Zhang, Melodie Galerne, Emilie Moulin, Felix Thomas Eickemeyer, Shaik M. Zakeeruddin, Jovana V. Milić, Nicolas Giuseppone,* and Michael Grätzel**

Hybrid perovskites stand out as one of the leading materials in the new generation of photovoltaics. Their stability under operating conditions, however, remains an ongoing challenge. In particular, aging at the interface with the charge transport materials contributes to the degradation during operation. To address this, functionalized triarylamine-based modulators are employed, which are known to form hole-transporting supramolecular stacks, at the interface between the perovskite active layer and the hole-transporting material in conventional perovskite solar cells. As a result, the improvements of the operational stabilities are demonstrated without compromising device performances, providing a promising strategy for advancing photovoltaics.

1. Introduction

Hybrid perovskite solar cells have reached remarkable performances over the past decade.[1] This has been, however, accompanied by limited stabilities under device operating conditions of voltage bias and light.[1–4] One of the main factors contributing to the limited stability during operation is ion migration, which can induce degradation processes, particularly at the interface with the selective charge-transport layers.[4–7] This is further pronounced for organic hole-transporting materials, such as the commonly employed 2,2′,7,7′-tetrakis[*N*,*N*-di(4-methoxyphenyl)amino]−9,9′-spirobifluorene (spiro-OMeTAD), which feature low conductivity in the order of 10^{-6} cm^2 V^{-1} s^{-1} that requires doping with metal salts, such as lithium bis(trifluoromethylsulfonyl)imide.[4,8–10] To prevent the detrimental ion migration across the interface,[5–7] the use of thin interlayers of molecular assemblies or graphene composites has been particularly effective.[2,4,11–14] However, most of these layers interfere with hole transport and often compromise the performances, stimulating the development of alternative strategies.[4]

Triarylamines (TAAs) are common constituents of hole-transporting materials in perovskite solar cells that feature superior durability[15] as well as the potential for interfacial passivation.[16,17] In addition, functionalized TAAs have the capacity to form supramolecular stacks, and it was shown that adding supplementary hydrogen bonding moieties, such as amide functions, enables assembling TAA molecules into highly organized supramolecular structures (**Figure 1**),[18–23] which can be doped by light or electrochemical activation.[18–21] Such partial oxidation of TAA results in an enhanced delocalization of charge carriers along the supramolecular wires with exceptional hole-transporting performances.[22,23] While other amide-based hole-transporting materials[24–26] and additives[27,28] have shown promise in perovskite photovoltaics, TAA-based assemblies have so far not been used as interfacial modulators in perovskite solar cells.

In this study, we have assembled TAA trisamides at the interface between hybrid perovskites and the hole-transport

M. Almalki, G. AlSabeh, M. A. Ruiz-Preciado, H. Zhang[+], F. T. Eickemeyer, S. M. Zakeeruddin, J. V. Milić, M. Grätzel
Laboratory of Photonics and Interfaces
Institute of Chemical Sciences and Engineering
École Polytechnique Fédérale de Lausanne
Lausanne 1015, Switzerland
E-mail: jovana.milic@unifr.ch; michael.graetzel@epfl.ch

G. AlSabeh, J. V. Milić
Adolphe Merkle Institute
University of Fribourg
Fribourg 1700, Switzerland

M. Galerne, E. Moulin, N. Giuseppone
SAMS research group
University of Strasbourg
CNRS
Institut Charles Sadron UPR22
Strasbourg 67000, France
E-mail: giuseppone@unistra.fr

The ORCID identification number(s) for the author(s) of this article can be found under https://doi.org/10.1002/admi.202301053

[+]Present address: The State Key Laboratory of Photovoltaic Science and Technology, Shanghai Frontiers Science Research Base of Intelligent Optoelectronics and Perception, Institute of Optoelectronics, Fudan University, Shanghai 200433, China

DOI: 10.1002/admi.202301053

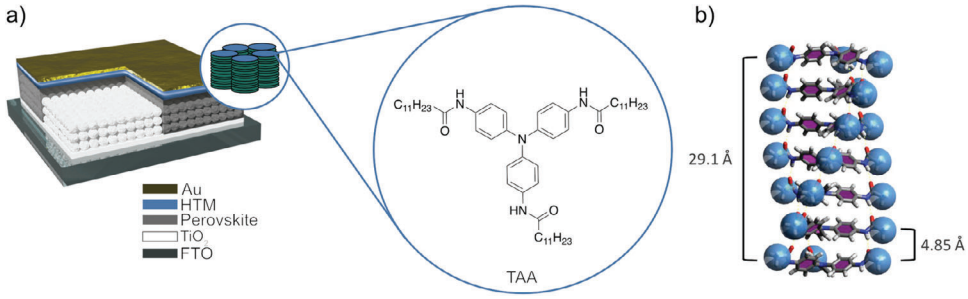

Figure 1. TAA modulation in perovskite solar cells. a) Schematic of a perovskite solar cell with the active layers and the structure of the triarylamine (TAA) employed in this study (n = 11) at the interface with the hole-transporting material (HTM). b) TAA self-assembly in a supramolecular stack.[22,23]

layers and investigated the structural and optoelectronic characteristics in thin films and perovskite solar cells. We obtain more operationally stable solar cells without compromising their resulting photovoltaic performances, offering a promising strategy for advancing material design in perovskite photovoltaics.

2. Results and Discussion

Films of hybrid perovskites based on the $FA_{0.97}MA_{0.03}Pb(I_{0.97}Br_{0.03})_3$ composition were deposited on glass substrates via two-step spin-coating in accordance with reported procedures, as described in the experimental section of the Supporting Information (Figures S1–S7).[29–31] We analyzed a series of TAA moieties functionalized with different alkyl chain lengths, identifying the modulators that are compatible with the use of orthogonal solvents for the preparation of thin films. In particular, only the TAA derivative with the longest alkyl chain length (n = 11, Figure 1a) demonstrated solubility in the appropriate solvents (i.e., chlorobenzene and 1,1,2,2-tetrachloroethane). This permitted modulation of the interface with the hole-transporting layer from the corresponding TAA solution in 1,1,2,2-tetrachloroethane in concentrations of 0.5 mg mL^{-1} followed by annealing for 10 min at 100 °C, as detailed in the experimental section. Hereafter, the pristine perovskite films or devices are referred to as the *control*, and TAA-treated (i.e., modulated) ones are abbreviated as *TAAT*.

The structural properties of the films were investigated by using X-ray diffraction (XRD; **Figure 2a**). XRD patterns of the TAAT films closely matched those of the control perovskites, suggesting comparable structural characteristics of the perovskite layer, which was corroborated by grazing incidence wide-angle X-ray scattering (GIWAXS) measurements (Figure S1, Supporting Information). This was further in accordance with the IR spectra (Figure S2, Supporting Information), suggesting weak interactions that do not alter the perovskite structural integrity. However, X-ray photoelectron spectroscopy (XPS) of the films revealed Pb $4f_{7/2}$ and $4f_{5/2}$ peaks at 138.77 and 143.66 eV, respectively, including additional signals at 136.98 and 141.83 eV for the control film that correspond to the metallic Pb^0. These signals were not observed in the treated films, suggesting that the TAA interacts with Pb on the surface (Figure 2b). The surface of the films was further assessed by scanning electron microscopy (SEM, Figure 2c–d and Figure S3, Supporting Information) and atomic force microscopy (AFM, Figure S4, Supporting Information), without a precise estimate of the thin TAA layer thickness, suggesting a comparable morphology in the presence of modulators even upon ultraviolet (UV) irradiation of the films.

In accordance with the structural and morphological characteristics, optical properties of hybrid perovskite thin films were not substantially affected by the presence of TAA moieties and their assemblies at the perovskite layer, as suggested by UV–vis absorption spectroscopy (Figure 2e). Moreover, the corresponding Tauc plots (Figure 2f) show a comparable optical bandgap of the TAA-modulated perovskite and the control samples of 1.54 eV, which is relevant for maintaining competitive photovoltaic performances of the resulting perovskite solar cells.

The photovoltaic performances were investigated in the conventional n-i-p device configuration of fluorine-doped tin oxide (FTO)/compact TiO_2 (≈60 nm)/ mesoporous (mp) TiO_2 (≈150 nm)/ perovskite (≈650 nm)/ spiro-OMeTAD (≈150 nm)/Au (≈80 nm) (Figure 1) with and without TAA at the interface between the perovskite and hole-transporting material (**Figure 3**, **Table 1**). To demonstrate the generality of the approach, we have also analyzed alternative $(FA_{0.9}MA_{0.1})_{0.95}Cs_{0.05}Pb_{1.03}(I_{0.93}Br_{0.1})_3$ perovskite compositions, showing an enhancement of the open-circuit voltage (V_{OC}) and the resulting power conversion efficiencies (Figure S6, Supporting Information), despite comparable structural and optoelectronic characteristics (Figure S7, Supporting Information). This is similar to the previous reports based on other amide additives,[27,28] leading to comparable performances of up to around 20% power conversion efficiency (PCE) for champion devices (19.8%; Table 1). Overall, TAA modulation resulted in comparable short circuit current density (*Jsc*) and fill factor (FF) across perovskite compositions, leading to an enhancement of photovoltaic metrics (Figure 3, Table 1, and Figures S5,S6, Supporting Information), which can be further optimized beyond the scope of this study.

To gain insights into the mode of action of TAA in perovskite devices, we conducted steady-state (SS) and time-resolved (TR) photoluminescence (PL) measurements.[32–34] TRPL measurements of control and TAAT films on glass showed a faster decay for TAAT compared to that of the control within the initial 50 ns (**Figure 4a**). By applying a mono-exponential fitting of TRPL curves, the decay time was estimated to be more than ten times faster for TAAT than that of the control films (Table S1, Supporting Information). This initial fast decay is a sign of hole injection from the perovskite film into TAA, suggesting

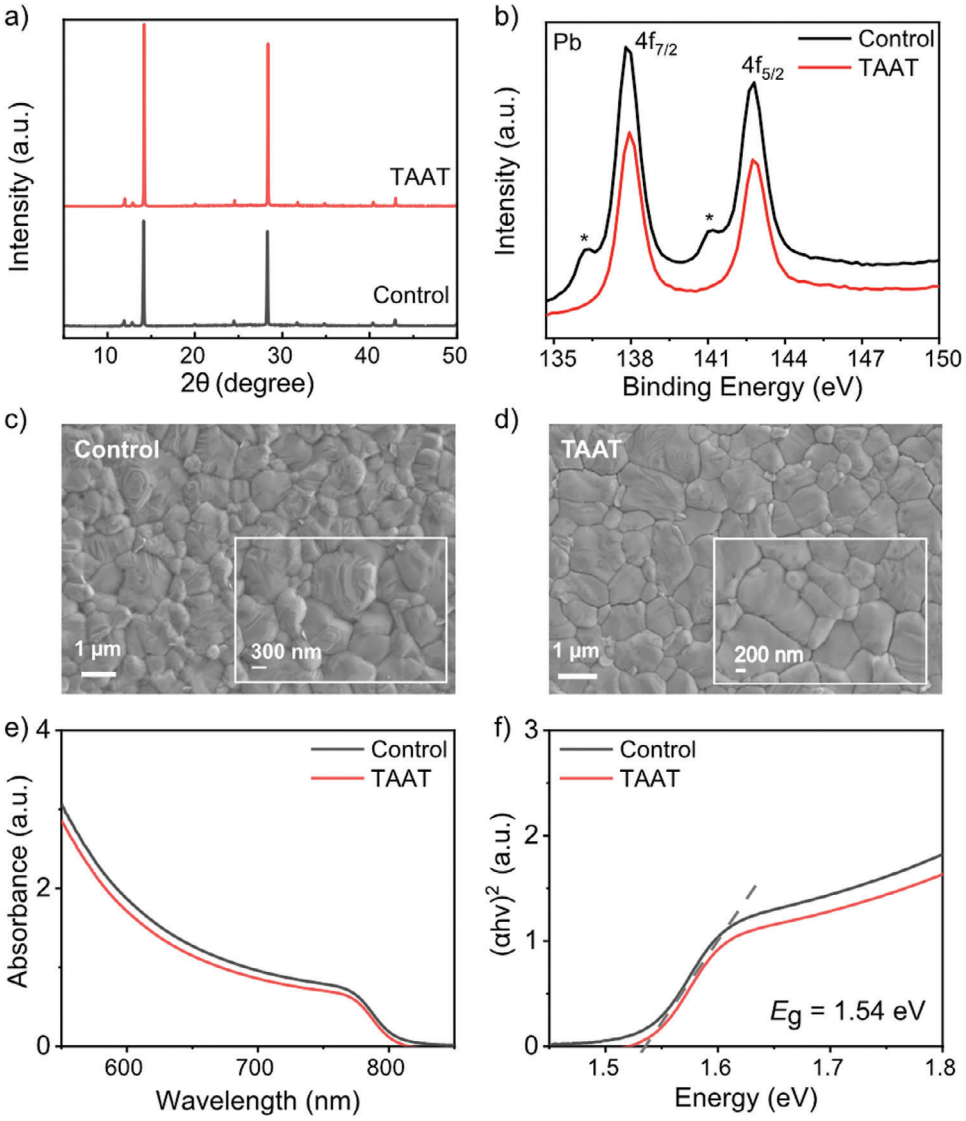

Figure 2. Effect of TAA-modulation (TAAT) on the properties of perovskite films. a) XRD patterns, b) Pb 4*f* core level XPS spectra (asterisk indicates the signals corresponding to the metallic lead, Pb^0), c–d) SEM images of thin films, and e) UV–vis absorption spectra, with f) the corresponding Tauc plots of the control (black) and TAAT (red) films on microscope glass slides with the energy bandgap (*Eg*) of 1.54 eV.

that TAA does not act as a barrier layer for charge extraction, which was in good agreement with the comparable device fill factor. Furthermore, the SSPL spectra revealed an emission peak at ≈ 800 nm, with a photoluminescence quantum yield (PLQY) of 4.5% for the control, which is an order of magnitude greater than that observed for the TAAT samples (0.4%; Figure 4b). This indicates a possible increase in non-radiative recombination losses at the interface of the perovskite film upon modulation, such as due to charge accumulation (i.e., holes in TAA and electrons in the perovskite layer). The introduction of spiro-OMeTAD led to comparable PL and PLQY (Figure 4c), suggesting that TAA does not increase non-radiative recombination in the device but acts as a charge-mediating transfer layer. This feature distinguishes TAA from other amide-based modulators applied to perovskite photovoltaics to date,[27,28] offering comparable performance (Table 1).

These changes in photovoltaic performances, however, suggest that supramolecular wiring was not likely to occur or play a substantial role under these experimental conditions, possibly due to an unfavorable orientation of TAA stacks at the interface, which requires further optimization. This would require better control of the morphology of the films and their orientation, such as through the use of alternative solvent systems to control the supramolecular assemblies.[18–21] Such modulation can nonetheless be relevant for the resulting operational stabilities that are primarily affected by the interface with the charge-selective transport layers. The stability of solar cells was thereby further investigated by monitoring the evolution of the performances under continuous operation. Unlike control devices, the modulated samples maintained over 80% of their performance for more than 1000 h, showing increased operational stability compared to the control (**Figure 5a**). This can be partly ascribed

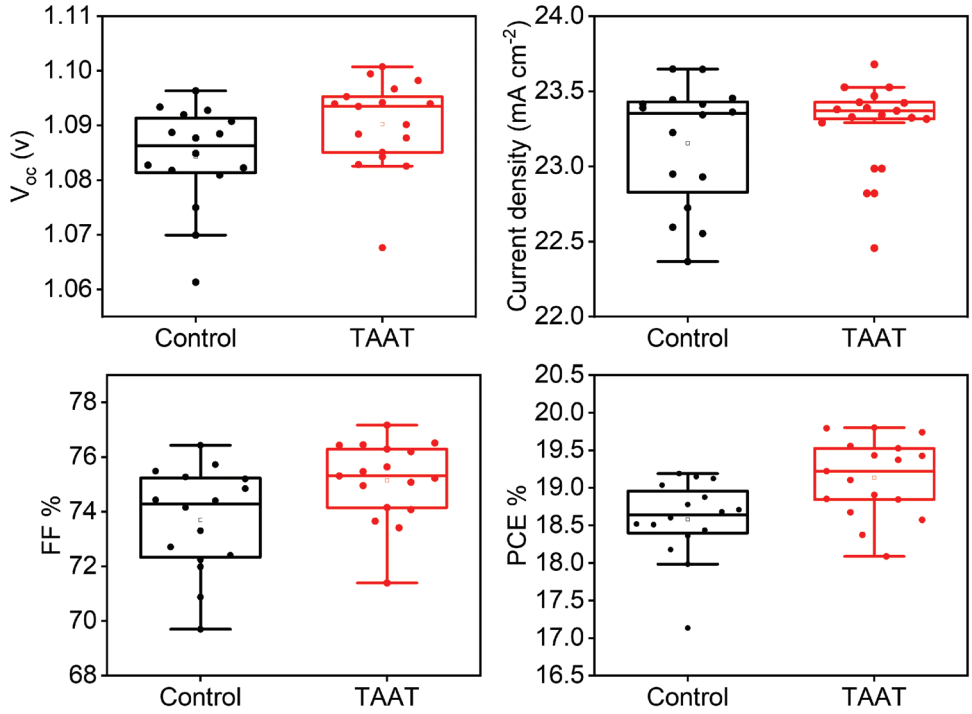

Figure 3. Photovoltaic device performance. Photovoltaic metrics of control (black) and TAAT (red) devices based on $FA_{0.97}MA_{0.03}Pb(I_{0.97}Br_{0.03})_3$ compositions. Experimental details with the representative *J-V* curves and performance metrics of other devices are shown in the Supporting Information (Figures S5–S7, Supporting Information).

to the increased hydrophobicity upon modulation, as suggested by contact angle measurements (Figure 5b), as well as improved contacts with the hole-transport layer that contribute to the overall stability.

In summary, we investigated the effect of triarylamine trisamide (TAA) derivatives as interfacial modulators between the perovskite absorber and hole-transporting layers in perovskite solar cells. We identified the contribution of the TAA modulators to interfacial charge extraction through a combination of techniques, including time-resolved photoluminescence and photoluminescence quantum yield spectroscopy, resulting in an enhancement of operational stabilities without compromising photovoltaic performances. This sets the stage for future advancements in designing electroactive (supra)molecular modulators in perovskite optoelectronics.

3. Experimental Section

N,N″,N‴-(nitrilotris(benzene-4,1-diyl))tritridecanamide (TAA) was prepared in accordance with the previously reported procedures.[19,35] A series of TAA derivatives of various sidechain lengths were considered (n = 1, 3, 8, 11; Figure 1a), and the one with solubility (0.5–1 mg mL^{-1}) in perovskite orthogonal solvents (chlorobenzene and 1,1,2,2-tetrachloroethane) was selected (n = 11, 0.5 mg mL^{-1}).

Materials: Titanium diisopropoxide bis(acetylacetonate) (75 wt% in isopropanol, Sigma-Aldrich); anhydrous ethanol (99.5%, Fischer Scientific); TiO_2 paste (Dyesol 30 NR-D); tin(IV) oxide colloidal dispersion (15% in water, Alfa Aesar); nickel nitrate hexahydrate ($Ni(NO_3)_2{\cdot}6H_2O$, 99.99%, Sigma Aldrich); 2- methoxyethanol (99%, Roth); [6,6]-Phenyl-C_{61}-butyric acid methyl ester ($PC_{61}BM$, Sigma Aldrich); chlorobenzene (CB, 99.8%, ACROS); bathocuproine (BC, 98%, TCI); spiro-OMeTAD (99%, Xi'an Polymer Light Technology Corp or Merck); lithium bis(trifluoro-methylsulphonyl)imide (LiTFSI, 99.95%, Sigma Aldrich); 4-*tert*-butylpyridine (4-tBP, 96%, Sigma-Aldrich); lead iodide (PbI_2, 99.9985%, Alfa Aesar); formamidinium iodide (FAI, 398%, Greatcellsolar); methylammonium iodide (MAI, 398%, Greatcellsolar); methylammonium chloride (MACl, 99%, Dyenamo); *N,N*-dimethylformamide (DMF, 99.8%, Acros); dimethyl sulfoxide (DMSO, 99.7%, Acros), α,α,α-trifluorotoluene (TFT, 99%, anhydrous, Sigma Aldrich).

Perovskite thin films were fabricated based on either $FA_{0.97}MA_{0.03}Pb(I_{0.97}Br_{0.03})_3$ (procedure 1) or $(FA_{0.9}MA_{0.1})_{0.95}Cs_{0.05}Pb_{1.03}(I_{0.93}Br_{0.1})_3$ (procedure 2) compositions, as specified in the description, by spin-coating the perovskite precursor solution on the substrates (specified in figure captions) through a stepwise preparation process reported previously.[30,31] The preparation was based on either procedure 1 or 2, as detailed below. A comparable procedure was used for the devices, complemented with the deposition of the hole-transporting layer and Au electrodes to complete the devices. Procedure 1 was primarily used for thin-film and device characterization and operational stability measurements (Figures 3–5; Figures S1–S5, Supporting Information), unless otherwise stated, whereas procedure 2 was applied to demonstrate the generality of the approach across compositions, with comparable

Table 1. Summary of average and champion device photovoltaic performance metrics.

Device		J_{SC} [mA cm^{-2}]	V_{OC} [V]	FF [%]	PCE [%]
Control	Average	23.2 ± 0.4	1.084 ± 0.009	74 ± 2	18.6 ± 0.5
	Champion	23.3	1.093	74	19.2
TAAT	Average	23.3 ± 0.3	1.090 ± 0.008	75 ± 1	19.1 ± 0.5
	Champion	23.5	1.101	76	19.8

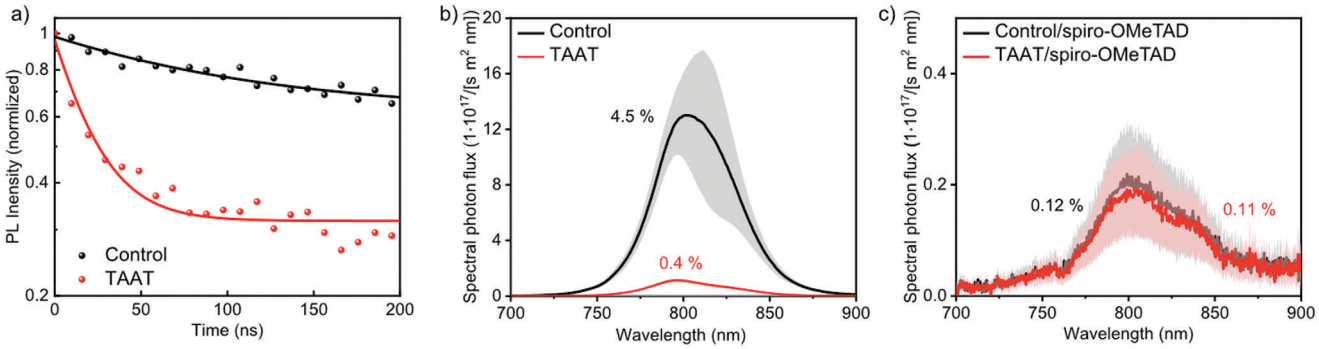

Figure 4. a) Time-resolved photoluminescence spectroscopy (TRPL) of perovskite (black) and TAA-modulated (TAAT, red) perovskite films on microscope glass slides. The solid lines indicate mono-exponential fit curves to the measured data (circles). Lifetimes are detailed in Table S1 (Supporting Information). b) Steady-state PL spectra of perovskite on glass (black) and TAA-modulated perovskite film on glass (red) on either (b) microscope glass slides or c) contact with the hole-transport material (spiro-OMeTAD). The error band represents the standard deviation of five samples per condition.

structural and optoelectronic characteristics (Figures S6,S7, Supporting Information).

Photovoltaic devices were fabricated using the n-i-p architecture with the constituent layers as follows: FTO/(40 nm) c-TiO_2/(250 nm) mp-TiO_2/(450 nm) perovskite/(180 nm) spiro-OMeTAD/(80 nm) Au based on the procedure reported previously.[30,31] An active area of 0.25 cm^2 (5 mm × 5 mm) was defined by the gold electrodes and a 0.16 cm^2 black metal mask was used during PV measurements to define the aperture area. For this purpose, glass sheets covered by FTO (Nippon sheet glass 8 Ω sq^{-1}) was thoroughly brushed with a 10% Hellmanex (Hellma GmbH) water solution and then placed under sonication in a 2% Hellmanex water solution for 30 min. After that, the Hellmanex solution was replaced by acetone and later ethanol and sonicated during 15 min and 10 min, respectively. Then, a ca. 40 nm-thick TiO_2 compact layer (c-TiO_2) was deposited by spray pyrolysis with a precursor solution of titanium diisopropoxide bis(acetylacetonate) (75 wt% in isopropanol) in anhydrous ethanol (99.5%) at 450 °C. After the spraying, the substrates were kept at 450 °C for 30 min. Then, a suspension of TiO_2 paste (Dyesol 30 NR-D) in ethanol was used to cast a ca. 250 nm-thick mesoporous TiO_2 (mp-TiO_2) layer by spin coating at 4000 rpm for 20 s with an acceleration of 2000 rpm s^{-1}. After the spin coating, the solvent was allowed to evaporate on a hot plate at 80 °C for 10 min and then sintered at 450 °C for 30 min under dry air flow. UV-ozone treatment for 15 min was used before the deposition of the c-TiO_2 and mp-TiO_2. A ca. 450 nm-thick perovskite layer was deposited on the substrates by spin coating following the antisolvent method to complete the solar cell devices based on either procedure 1 or 2.

Procedure 1: The perovskite layer was deposited using a single-step deposition method from a precursor solution based on $FA_{0.97}MA_{0.03}Pb(I_{0.97}Br_{0.03})_3$ composition.[31] The solution was prepared in Ar atmosphere by dissolving PbI_2 (1.51 M), FAI (1.47 M), and MABr (0.03 M), $PbBr_2$ (0.03 M) and MACl (0.6 M) in anhydrous DMF/DMSO (4:1 (v:v)). The precursor solution was spin-coated onto the mesoporous TiO_2 films in a one-step program at 600 and 5000 rpm for 30 s. CB of 200 µl was dropped on the spinning substrate 10 s prior the end of the program. This was followed by annealing the films at 150 °C for 10 min. The substrates were cooled down to room temperature before depositing 100 µL of TAA solution in 1,1,2,2-tetrachloroethane (0.5–1 mg mL^{-1}) on the substrates while they were spin-coated at 5000 rpm for 30 sec and heated at 100 °C for 5 min. For completing the fabrication of devices, HTM was deposited onto perovskite films by spin-coating at 4000 rpm for 20 s. HTL involved 90 mg of spiro-OMeTAD doped with LiTFSI (17.8 µl prepared by dissolving 520 mg LiTFSI in 1 mL of acetonitrile) and 28.8 µl of 4-tBP dissolved in 1 mL of CB. Finally, ≈80 nm gold layer was thermally evaporated as contact electrodes to complete the devices.

Procedure 2: The precursor perovskite solution based on $(FA_{0.9}MA_{0.1})_{0.95}Cs_{0.05}Pb_{1.03}(I_{0.93}Br_{0.1})_3$ composition was drop-casted on the substrates and spun at 2000 rpm (200 rpm s^{-1} acceleration) and 6000 rpm (acceleration of 2000 rpm s^{-1}) for 10 s and 30 s, respectively.[30] During the last 10 s of the second spin-coating step, 220 µL of the TFT antisolvent was drop-casted. The perovskite film was then dried on a hot plate at 100 °C for 60 min. The substrates were allowed to cool down for 10 min. A 60 µL of the solution of TAA of the concentration of 0.5–1 mg mL^{-1} dissolved in 1,1,2,2-tetrachloroethane was deposited onto the perovskite film, which was followed by spin-coating at 5000 rpm for 30 sec and heating at 80 °C for 10 min. A 70 mM solution of spiro-OMeTAD in CB was prepared. LiTFSI and 4-tBP were used as additives in a 0.5 and 3.3 mol% (relative to spiro-OMeTAD), respectively. This solution was spin-coated on the perovskite film at 2000 rpm (acceleration of 1200 rpm s^{-1}) for 20 s to form a ca. 180 nm HTL. The perovskite and spiro-OMeTAD layers were deposited in a dry air glovebox. In the final step, 80 nm gold electrodes were deposited by thermal evaporation.

Attenuated total reflection Fourier Transform Infrared spectroscopy (ATR-FTIR) was measured with Nicolet 6700 from ThermoFisher Scientific with ATR obtained with the golden gate accessory from Specac.

X-ray diffraction (XRD) patterns were recorded on an X'Pert MPD PRO (PANanalytical) equipped with a ceramic tube providing Ni-filtered (Cu anode, λ = 1.54060 Å) radiation and a RTMS X'Celerator (PANalytical). The measurements were done in BRAGG-BRENTANO geometry from 2θ = 5–60°. The samples were mounted without further modification, and the automatic divergence slit (10 mm) and beam mask (10 mm) were adjusted to the dimension of the films. More information is available under the https://doi.org/10.15151/ESRF-ES-1021690577. *GIWAXS measurements* were performed at the ESRF SNBL BM01 beamline.

UV–vis absorption measurements were recorded using Varian Cary5 UV–vis spectrophotometer.

Steady-state photoluminescence (PL) spectra were recorded by exciting the perovskite films deposited onto microscope glass. The emission between was recorded with a Fluorolog 322 spectrometer (Horiba Jobin Yvon iHr320 and a CCD). The samples were mounted at 60° and emission was recorded at 90° from the incident beam path.

Time-resolved photoluminescence (TRPL) was measured via time-correlated single photon counting (TCSPC) using a LifeSpec II (Edinburgh Instruments) fluorescence spectrometer with a picosecond pulsed diode laser (EPL-510, Edinburgh Instruments) at 510 nm and 85 ps pulse width.

Photoluminescence quantum yield (PLQY) was measured using an integrating sphere (Fluorolog, Horiba JobinYvon), an Andor Kymera 193i spectrograph, and a 660 nm continuous-wave laser (OBIS, Coherent) set at 1-Sun equivalent photon flux (1.1 µm beam full-width half-maximum, 632 µW); photoluminescence was collected at normal incidence using a 0.1 NA, 110 µm-diameter optical fiber.[33] For the absolute spectral calibration of the PLQY measurement system, a radiometrically calibrated halogen lamp (HL-3 plus CAL from Ocean Optics) was used.

Current-voltage characteristics of pristine (control) as well as the modulated perovskite layer-based PSCs were obtained under standard AM 1.5G illumination at a light intensity of 100 mW cm^{-2}. The J-V curves were

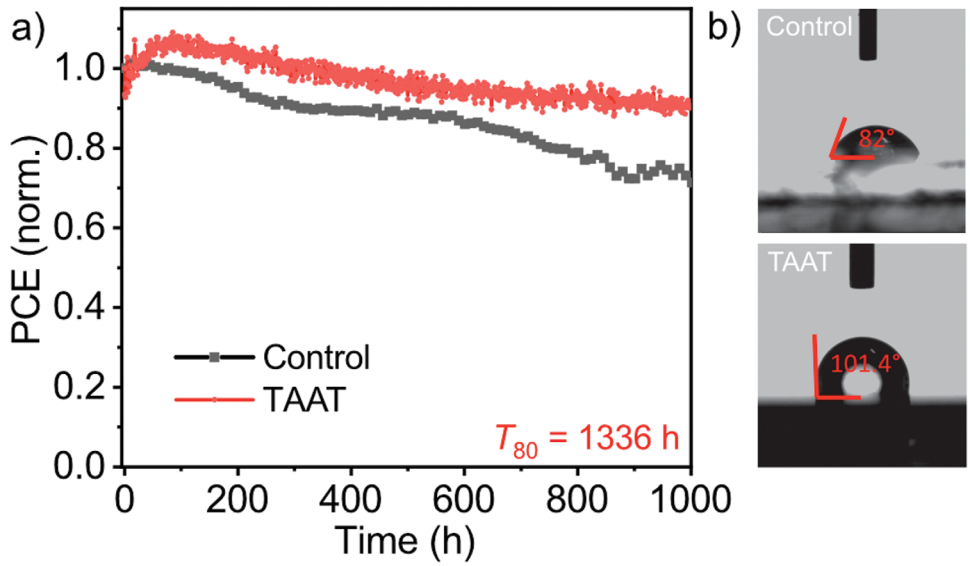

Figure 5. Operational stability of perovskite devices. a) Maximum power point tracking evolution of the unencapsulated device under full solar illumination (AM 1.5 G, 100 mW cm^{-2} under nitrogen at 25 °C). The time to reach 80% of initial power conversion efficiency (T_{80}) is extrapolated for modulated samples for comparison. b) Contact angle measurements with a water droplet with control (top) and TAAT (bottom) films.

recorded at a scanning rate of 50 mV s^{-1} under standard AM 1.5G solar radiation and reverse bias (from V_{OC} to J_{SC}).

Incident photon-to-current efficiency (IPCE) was recorded with a commercial apparatus (Aekeo-Ariadne, Cicci Research s.r.l.) based on a 300-W Xenon lamp.

Contact angle measurements were recorded with a drop shape analyzer (KRÜSS, DSA100) at ambient temperature to assess hydrophilicity of surfaces.

X-Ray Photoelectron Spectroscopy (XPS) measurements were carried out using a PHI VersaProbe II scanning XPS microprobe (Physical Instruments AG, Germany).

Operational stability measurements were performed on complete devices using Fluxim Litos Lite system by monitoring maximum power point under N_2 atmosphere at ambient temperature.

Supporting Information

Supporting Information is available from the Wiley Online Library or from the author.

Acknowledgements

The project has received support from the EU Horizon 2020 research and innovation program under grant agreement No. 764047. G.A. and J.V.M. acknowledge the SNSF Grant (193174). M.A. acknowledges King Abdulaziz City for Science and Technology (KACST) for the fellowship. The authors were grateful to Dr. Olivier Ouellette (EPFL) for support with the PL spectroscopy and to Dr. Alexander Hinderhofer, Lena Merten, Paul Zimmermann, and Frank Schreiber (University of Tübingen) for their support during the synchrotron-based X-ray scattering measurements. The authors were further grateful to the ESRF (proposal no. a0121290) for the synchrotron-based measurements and Dmitry Chernyshov, in particular, for their invaluable support.

Conflict of Interest

The authors declare no conflict of interest.

Author Contributions

M.A. and G.A. contributed equally to this work. The project was conceptualized by J.V.M. with the support of N.G., who supervised the synthesis and characterization of the wires by M.G. and E.M., while M.A., G.A., H.Z., and M.A.R.-P. fabricated and characterized perovskite materials and devices. F.E. performed the PL characterizations and the analysis. S.M.Z. was involved in the discussion, whereas M.G. directed the study. All the authors contributed to the manuscript.

Data Availability Statement

The datasets are available from the first author upon request. Data presented here can also be accessed at the following https://doi.org/10.5281/zenodo.10779480, and it is available under the license CC-BY-4.0 (Creative Commons Attribution-ShareAlike 4.0 International). The ESRF data is available under the doi: 10.15151/ESRF-ES-1021690577 dataset.

Keywords

hybrid perovskite photovoltaics, molecular charge transport, supramolecular modulation, triarylamine

Received: December 13, 2023
Revised: January 29, 2024
Published online:

[1] A. K. Jena, A. Kulkarni, T. Miyasaka, *Chem. Rev.* **2019**, *119*, 3036.
[2] R. Wang, M. Mujahid, Y. Duan, Z.-K. Wang, J. Xue, Y. Yang, *Adv. Funct. Mater.* **2019**, *29*, 1808843.
[3] M. V. Khenkin, E. A. Katz, A. Abate, G. Bardizza, J. J. Berry, C. Brabec, F. Brunetti, V. Bulović, Q. Burlingame, A. Di Carlo, R. Cheacharoen, Y.-B. Cheng, A. Colsmann, S. Cros, K. Domanski, M. Dusza, C. J. Fell, S. R. Forrest, Y. Galagan, D. Di Girolamo, M. Grätzel, A. Hagfeldt, E. Hauff, H. Hoppe, J. Kettle, H. Köbler, M. S. Leite, S. F. Liu, Y.-L. Loo, J. M. Luther, et al., *Nat. Energy* **2020**, *5*, 35.

[4] J. Wei, Q. Wang, J. Huo, F. Gao, Z. Gan, Q. Zhao, H. Li, *Adv. Energy Mater.* **2020**, *77*, 2002326.
[5] K. Domanski, J.-P. Correa-Baena, N. Mine, M. K. Nazeeruddin, A. Abate, M. Saliba, W. Tress, A. Hagfeldt, M. Grätzel, *ACS Nano* **2016**, *10*, 6306.
[6] K. Domanski, B. Roose, T. Matsui, M. Saliba, S.-H. Turren-Cruz, J.-P. Correa-Baena, C. R. Carmona, G. Richardson, J. M. Foster, F. De Angelis, J. M. Ball, A. Petrozza, N. Mine, M. K. Nazeeruddin, W. Tress, M. Grätzel, U. Steiner, A. Hagfeldt, A. Abate, *Energy Environ. Sci.* **2017**, *10*, 604.
[7] K. Domanski, E. A. Alharbi, A. Hagfeldt, M. Grätzel, W. Tress, *Nat. Energy* **2018**, *3*, 61.
[8] J.-Y. Seo, S. Akin, M. Zalibera, M. A. R. Preciado, H.-S. Kim, S. M. Zakeeruddin, J. V. Milić, M. Grätzel, *Adv. Funct. Mater.* **2021**, *31*, 2102124.
[9] R. L. Forward, K. Y. Chen, D. M. Weekes, D. J. Dvorak, Y. Cao, C. P. Berlinguette, *ACS Energy Lett.* **2019**, *4*, 2547.
[10] G. W. Kim, H. Choi, M. Kim, J. Lee, S. Y. Son, T. Park, *Adv. Energy Mater.* **2020**, *10*, 1903403.
[11] J. V. Milić, N. Arora, M. I. Dar, S. M. Zakeeruddin, M. Grätzel, *Adv. Mater. Interfaces* **2018**, *356*, 1800416.
[12] J. V. Milic, *J. Mater. Chem. C* **2021**, *9*, 11428.
[13] S. Shao, M. A. Loi, *Adv. Mater. Interfaces* **2019**, *7*, 1901469.
[14] S. Y. Kim, S. J. Cho, S. E. Byeon, X. He, H. J. Yoon, *Adv. Energy Mater.* **2020**, *131*, 2002606.
[15] J. Wang, K. Liu, L. Ma, X. Zhan, *Chem. Rev.* **2016**, *116*, 14675.
[16] M. Wang, H. Wang, W. Li, X. Hu, K. Sun, Z. Zang, *J. Mater. Chem. A* **2019**, *7*, 26421.
[17] Y. Fu, Y. Li, G. Xing, D. Cao, *Mater. Today Adv.* **2022**, *16*, 100300.
[18] V. Faramarzi, F. Niess, E. Moulin, M. Maaloum, J.-F. Dayen, J.-B. Beaufrand, S. Zanettini, B. Doudin, N. Giuseppone, *Nat. Chem.* **2012**, *4*, 485.
[19] J. J. Armao IV, M. Maaloum, T. Ellis, G. Fuks, M. Rawiso, E. Moulin, N. Giuseppone, *J. Am. Chem. Soc.* **2014**, *136*, 11382.
[20] J. J. Armao IV, Y. Domoto, T. Umehara, M. Maaloum, C. Contal, G. Fuks, E. Moulin, G. Decher, N. Javahiraly, N. Giuseppone, *ACS Nano* **2016**, *10*, 2082.
[21] T. K. Ellis, M. Galerne, J. J. Armao IV, A. Osypenko, D. Martel, M. Maaloum, G. Fuks, O. Gavat, E. Moulin, N. Giuseppone, *Angew. Chem., Int. Ed.* **2018**, *57*, 15749.
[22] E. Moulin, J.-J. Cid, N. Giuseppone, *Adv. Mater.* **2012**, *25*, 477.
[23] E. Moulin, J. J. Armao IV, N. Giuseppone, *Acc. Chem. Res.* **2019**, *52*, 975.
[24] M. L. Petrus, K. Schutt, M. T. Sirtl, E. M. Hutter, A. C. Closs, J. M. Ball, J. C. Bijleveld, A. Petrozza, T. Bein, T. J. Dingemans, T. J. Savenije, H. Snaith, P. Docampo, *Adv. Energy Mater.* **2018**, *8*, 1801605.
[25] S.-Y. Wang, C.-P. Chen, C.-L. Chung, C.-W. Hsu, H.-L. Hsu, T.-H. Wu, J.-Y. Zhuang, C.-J. Chang, H. M. Chen, Y. J. Chang, *ACS Appl. Mater. Interfaces* **2019**, *11*, 40050.
[26] M. M. H. Desoky, M. Bonomo, R. Buscaino, A. Fin, G. Viscardi, C. Barolo, P. Quagliotto, *Energies* **2021**, *14*, 2279.
[27] J. Xie, Z. Zhou, H. Qiao, M. Chen, L. Wang, S. Yang, Y. Hou, H. Yang, *J. Energy. Chem.* **2021**, *56*, 179.
[28] Y. Zhang, J. Xie, L. Tao, B. Jiang, S. Ma, W. Kong, J. Zhang, H. Wang, *Org. Electron.* **2022**, *108*, 106597.
[29] J. V. Milić, J.-H. Im, D. J. Kubicki, A. Ummadisingu, J.-Y. Seo, Y. Li, M. A. Ruiz Preciado, M. I. Dar, S. M. Zakeeruddin, L. Emsley, M. Grätzel, *Adv. Energy Mater.* **2019**, *131*, 1900284.
[30] M. A. Ruiz Preciado, D. J. Kubicki, A. Hofstetter, L. McGovern, M. H. Futscher, A. Ummadisingu, R. Gershoni-Poranne, S. M. Zakeeruddin, B. Ehrler, L. Emsley, J. V. Milić, M. Grätzel, *J. Am. Chem. Soc.* **2020**, *142*, 1645.
[31] T.-S. Su, F. T. Eickemeyer, M. A. Hope, F. Jahanbakhshi, M. Mladenović, J. Li, Z. Zhou, A. Mishra, J.-H. Yum, D. Ren, A. Krishna, O. Ouellette, T.-C. Wei, H. Zhou, H.-H. Huang, M. D. Mensi, K. Sivula, S. M. Zakeeruddin, J. V. Milić, A. Hagfeldt, U. Rothlisberger, L. Emsley, H. Zhang, M. Grätzel, *J. Am. Chem. Soc.* **2020**, *142*, 19980.
[32] L. Krückemeier, U. Rau, M. Stolterfoht, T. Kirchartz, *Adv. Energy Mater.* **2020**, *10*, 1902573.
[33] T. Kirchartz, J. A. Márquez, M. Stolterfoht, T. Unold, *Adv. Energy Mater.* **2020**, *10*, 1904134.
[34] S. You, F. T. Eickemeyer, J. Gao, J.-H. Yum, X. Zheng, D. Ren, M. Xia, R. Guo, Y. Rong, S. M. Zakeeruddin, K. Sivula, J. Tang, Z. Shen, X. Li, M. Grätzel, *Nat. Energy* **2023**, *8*, 515.
[35] A. Osypenko, E. Moulin, O. Gavat, G. Fuks, M. Maaloum, M. A. J. Koenis, W. J. Buma, N. Giuseppone, *Chem. – A Eur. J.* **2019**, *25*, 13008.